Spectroscopic Properties Unique to Nano-Emitters

Andrew G. Walsh,[†,‡,§] Wolfgang Bacsa,[¶]
A. Nickolas Vamivakas,[⊥,‡,∥] and Anna K. Swan*,[⊥,†,‡]

Department of Physics, 590 Commonwealth Avenue, and Department of Electrical and Computer Engineering and The Boston University Photonics Center, 8 Saint Mary's Street, Boston University, Boston, Massachusetts 02215, and CEMES UPR-CNRS, 29 rue Jeanne Marvig, Université Toulouse, 31055 Toulouse, France

ABSTRACT

The spectral position of light emission from an individual carbon nanotube is shown to depend on the location of the nanotube within the focal spot, while no such effect is present for macroscopic emitters. In addition, in contrast to macroscopic emitters, the measured line width from the nanotube emitter is independent of spectrometer entrance slit width. The effects are general for any nanoscale optical emitter with at least one dimension smaller than the optical diffraction limit.

Optical microscopy and spectroscopy are ubiquitous tools in the rapidly evolving area of nanoscience and nanotechnology. The optical resolution of standard confocal microscopy limits the resolution to a volume much larger than a nanoscale object, and ensemble measurements are often used to demonstrate the overall behavior of nanoscale systems. However, spectroscopy of individual nanoscale objects provides specific information that is not always apparent in ensemble measurements. Spectroscopy of individual nanoparticles is most easily achieved by diluting the number of emitters in the focal spot to less than one. The spectroscopic signature of the individual emitter can be used for identification, e.g., the size of a quantum dot,[1] or to probe shifts of electronic levels as a function of electric field,[2,3] magnetic field,[4,6] temperature,[7] strain,[8-10] dielectric environment,[11,12] or other external perturbations. The need to make measurements from individual nanoemitters has proved to be especially important for carbon nanotubes, since samples consisting of only one (n,m) species is difficult to attain,[13,14] and CNTs belonging to different families often feature opposed response to perturbations, e.g., strain.[8,9] In this paper, we demonstrate two spectroscopic features that are unique to individual nanoemitters: the measured spectral position depends on the position of the nanoemitter in the focal spot; and the measured line width is completely independent of

spectrometer entrance slit width. The link between nanoemitter position and spectral readout could lead to misinterpretation of the collected spectral signature; e.g., photoluminescence from a diffusing colloidal quantum dot could be interpreted as spectral wandering or a wider natural line width, depending on the collection time scale. For a stationary carbon nanotube slightly off axis in the focal spot, the resulting spectral shift of the Raman radial breathing mode[15] could lead to misidentification of the (n,m) species. On the other hand, if the spectral signature is known, one can use the spectral information to pinpoint the location of the nanoparticle along one direction to a fraction of the diffraction limited focal spot. The results we demonstrate here are generally valid for any system with at least one dimension in the nanoscale, e.g., quantum dots and nanoparticles, nanotubes and nanorods, and even two-dimensional quantum wells if imaged on their sides, projecting a 1D line. Here, we use Raman scattering from a carbon nanotube to experimentally demonstrate effects unique to spectroscopy of an object smaller than the focal spot.

Central to the understanding of the link between physical position and spectral signature is the concept of mapping, and we therefore consider a microscope−spectrometer system with two infinity-corrected imaging lens systems; the object plane is imaged to spectrometer entrance slit, and the second lens system images the intermediate image plane of the entrance slit to the spectrometer charge coupled detector (CCD) (Figure 1a). The magnifications of the two imaging systems are M_{OS} and M_{SD}, respectively. The grating is oriented so as to diffract the light of wavelength λ_0 emanating from the nanoemitter located at the focal point of the object

* Corresponding author. E-mail: swan@bu.edu.
† Department of Physics, BU.
‡ The Boston University Photonics Center.
§ Now at MTPV Corporation, Boston, MA.
¶ CEMES UPR-CNRS, Universite Toulouse.
⊥ Department of Electrical and Computer Engineering, BU.
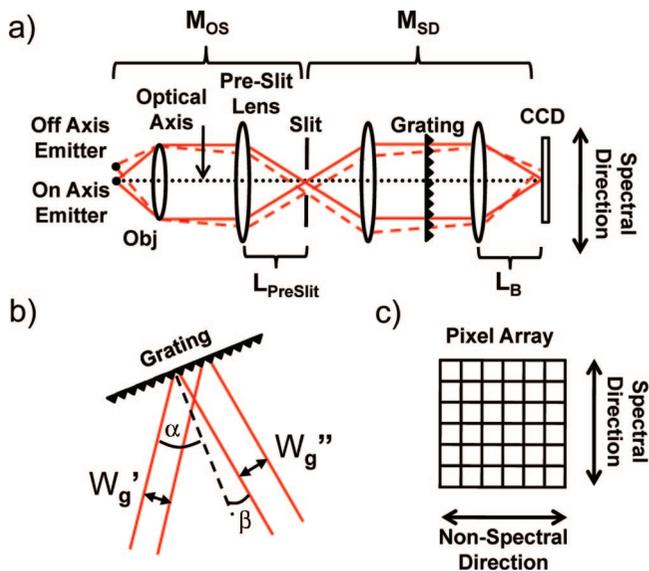∥ Now at Cavendish Laboratory, University of Cambridge, UK.

Figure 1. Schematic of a microscope−spectrometer setup with two infinity-corrected imaging lens systems. (a) Ray traces for emission of the same wavelength λ_0 from on-axis (solid red line) and off-optical axis (dashed red line) locations illustrating the effect of false spectral shifts from off-optical axis emission from a nanoemitter. (b) Close up of the grating and associated beam angles and widths. (c) CCD pixel array, showing the spectral and nonspectral directions defined by the grating orientation.

plane to the center position of the detector. For the purpose of highlighting the similarities to imaging, the grating is displayed as a transmission grating, with the diffraction angle not shown in the schematic in Figure 1a. W'_g and W''_g are the widths of the light beam incident and diffracted from the grating, respectively, which depend on the entrance angle and diffraction angle with respect to the grating normal, as shown in Figure 1b. The system is assumed to be properly aligned and calibrated so that the illumination is exactly in focus and along the optical axis. Furthermore, we will assume that the system is aberration free.[16] The presence of the grating in the second imaging system maps and disperses the light in the direction defined as the "spectral direction" perpendicular to the groves, and maps onto the nonspectral direction parallel to the grooves, as shown in Figure 1c. The spectral and nonspectral directions are imaged onto the object plane of the microscope as well as the intermediate image plane. In this paper we are only concerned with displacements in the spectral direction.

Figure 1a qualitatively illustrates the effects of off-optical axis emission. Rays from on-axis emitter with emission wavelength λ_0 are traced in solid line. With the emitter displaced to an off-axis location, the emission is mapped on different area on the detector (dashed lines), even though the same wavelength λ_0 is emitted. Specifically, a displacement in the object plane Δx_{obj} is imaged to a displacement at the slit, $\Delta x_{slit} = \Delta x_{obj} M_{OS}$. The second path both magnifies and disperses the light. The physical displacement on the CCD is recorded as a change in wavelength. Hence we can calculate the shift in spectral position $\Delta\sigma$ due to a displacement Δx_{obj} of the nanoemitter from the optical axis along the spectral direction,[17]

$$\Delta\sigma = \Delta x_{obj} M_{OS} M_{SD} \, d\sigma/dx \qquad (1)$$

where $\Delta\sigma$ is the shift in cm^{-1} due to displacement Δx_{obj} and the linear dispersion $d\sigma/dx = \lambda^{-2}\cos(\beta)/knL_B$ is calculated from the wavelength λ, grating order k, groove density n, exit focal length L_B and exit angle β.

The effect is readily verified. Our particular nanoemitter is a single, resonant carbon nanotube (CNT) suspended across a gap of ~20 μm. Incident supercontinuum light is focused onto the gap from the side with a second objective in a dark field configuration to locate the CNT and to align the sample. The sample is shown in Figure 2a with the CNT visible upon supercontinuum illumination.[18,19] The diameter of the CNT is approximately 1.5 nm, well below the optical diffraction limit and thus can be treated as an ideal point source emitter in the direction orthogonal to the nanotube axis. Furthermore, there are no other emitters in the diffraction limited excitation focal spot.

Extended sources with some degree of coherence can also exhibit spectral distortion within the envelope of the emission spectrum.[20] The spectral distortion in this case is not because the light is imaged to the wrong point on the spectrometer, but is due to interference in mapping the source spectrum to the detector. In our case, where we are using a nanotube aligned along the nonspectral direction, interference due to overlap within the point spread function is possible. Additionally, substantial spectral variations in the measured spectrum may be observed in the neighborhood of locations where the focused electric field has a null.[21] Here, we are ignoring such effects and treating the Raman emission from different points on the nanotube as incoherent and removed from regions of focal field nulls.

For this study, single line 820 nm laser light (continuous wave Ti-Sapphire laser, ~0.5 mW) in reflection mode is used to excite the nanotube Raman active G$^+$ mode at 1590 cm^{-1} shift ($\lambda_0 = 943$ nm). The lower right inset of Figure 2a shows the two excitation paths. The upper left inset of Figure 2a shows the intensity of the Raman signal as a function of
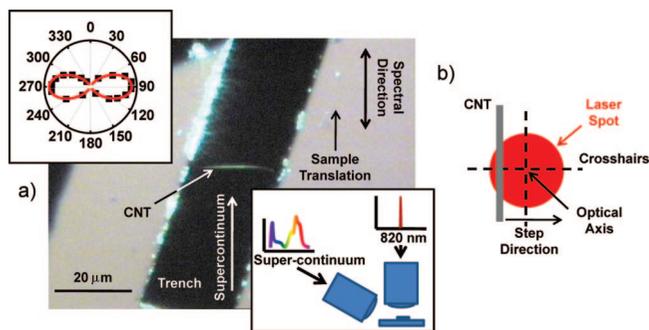

Figure 2. (a) Optical image of a single suspended CNT using supercontinuum illumination. The incident supercontinuum direction is as shown, inclined approximately 30° from the sample plane. The spectral direction, mapped from the CCD back into the object plane, is shown as well. The sample is translated parallel to the spectral direction. Lower right inset: Schematic of single line (820 nm) illumination and side illumination by the supercontinuum. Upper left inset: Polar plot of the G$^+$ Raman mode intensity, collected in reflection geometry, as a function of incident polarization. (b) Geometry of the CNT being translated through the laser illumination spot along the spectral direction.
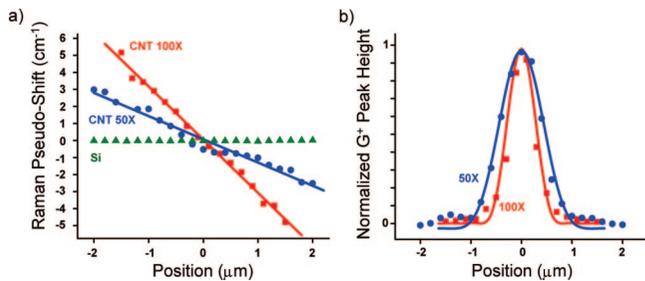
Figure 3. (a) Measured Raman shifts using both the $100\times/0.9$ NA objective (red squares) and $50\times/0.5$ NA objective (blue circles). The measured and calculated slopes for the $50\times/0.5$ NA objective were -1.36 and -1.50 cm$^{-1}/\mu$m, respectively, and -3.12 and -3.00 cm$^{-1}/\mu$m for the $100\times/0.9$ NA objective. For the extended emitter (Si 520 cm^{-1} Raman mode, green triangles) there is no effect. (b) Profiles of the laser spot focused by the $100\times/0.9$ NA and $50\times/0.5$ NA objectives, shown in blue and red lines, respectively, as measured by the CNT. Calculated ASR model results for a 1.46 mm Gaussian beam incident on the objective back aperture[23] are shown with solid lines. The measured FWHM for the $50\times/0.5$ NA and $100\times/0.9$ NA are 0.95 and 0.54 μm, respectively.

polarization angle of the incident laser, illustrating the strong directional polarization effect of the CNT,[22] and verifies the polarization direction of the incident light. The incident light is polarized along the CNT axis for maximum signal.

The CNT is translated in 200 nm steps ($\sim\lambda_0/5$) along spectral direction through the focal spot of the CW laser, collecting G$^+$ Raman mode spectra at each step, as depicted in Figure 2b. The spectral position of the G$^+$ Raman mode is plotted against spatial position of the nanotube and clearly shows the linear correlation between spatial location and spectroscopic shift. The dispersion using a $100\times/0.9$ NA objective is shown with red squares in Figure 3a. The dispersion is twice that obtained using a $50\times/0.5$ NA objective, shown in blue circles. The factor of 2 difference in dispersion is due to the factor of 2 difference in M_{OS} as expected from eq 1. The maximum measured shift in wavenumber is ±5 cm^{-1} corresponding to ±1.5 μm displacement. In order to limit such spectral uncertainty, the spectrometer slit should be closed to limit collection to a confocal area, or a confocal collection fiber can be used to couple light into the spectrometer.[24] However, even a displacement within the FWHM of the focal spot intensity (±280 nm) gives a ~2 cm^{-1} variation. We note that in the CNT literature, there is a variation of the reported values of Raman G$^+$ band of several wavenumbers. The G$^+$ band frequency is affected by strain,[8,9] temperature, and charging[25,26] effects. Our results show that the location of the nanotube is also a factor to be considered.

Raman spectroscopy is generally more forgiving of alignment issues than, e.g., photoluminescence, since a relative shift between Raman peak and laser line is measured. However, we note here that if the laser line scatters from

the substrate surface in the focal spot, it still will be centered at the correct CCD pixel, while the emission from an off-center nanoemitter will be displaced.

The dispersion is calculated using eq 1 and shows good agreement with the measurements. The parameter values for our spectrometer are listed in Table 1. Since the center position, and hence the true wavelength, can be determined with the help of the intensity profile discussed below, it is possible to use the spectral information to locate the nanoemitter relative to the optical axis to better than the diffraction limit. We consider the $100\times/0.9$ NA objective, which collects more light and hence gives a better signal-to-noise ratio than the $50\times/0.5$ NA objective. From peak fitting, the spectral position is determined, conservatively, to a precision of better than a quarter of a wavenumber. Using the measured linear dispersion of 3.1 cm$^{-1}/\mu$m, the position of the nanotube can be determined to 80 nm precision, or $\sim\lambda/12$. We note that with emitters of known and nonoverlapping spectral signatures, the distance between emitters in the spectral direction can then also be determined with similar subwavelength precision. Higher magnifications M_{OS} and M_{SD} increase the sensitivity to position. The linear dispersion is inversely proportional to the number of grooves, so a more dispersive grating will decrease the linear dispersion and hence decrease the sensitivity. However, it will also provide more data points of the spectral feature and can therefore provide a more precise determination of the measured spectral position.

We also show in green triangles in Figure 3a the absence of any spectral shift for an extended emitter, in this case the 520 cm^{-1} Raman line of silicon. This is to be expected since silicon is translationally invariant. Here, the off-axis emission will just act to broaden the natural line width of the spectral feature. Neither are spectral shifts from ensemble measurements of nanoemitters to be expected, only a slit width dependent broadening.

A nanoemitter can readily be used to directly measure the focusing objective excitation spot profile. The intensity of the G$^+$ Raman mode is plotted as a function of sample position for both a $100\times/0.9$ NA and a $50\times/0.5$ NA objective in Figure 3b. Data are compared to model calculations using a full vector treatment using the angular spectrum representation (ASR),[27] shown as solid lines in Figure 3b. The measured data matches the ASR results to within 5% and yields FWHMs of 0.96 and 0.54 μm for the $50\times/0.5$ NA and $100\times/0.9$ NA objectives, respectively. For comparison, the standard Rayleigh criterion $0.61\lambda/\text{NA}$[28] yields 1.00 and 0.56 μm for the $50\times/0.5$ NA and $100\times/0.9$ NA objectives.

The last point we make is that a nanoemitter acts as a "nano-slit." The measured line width is not broadened by opening up the spectrometer slit width, since the nanoemitter is imaged on the entrance slit with the smallest possible spot size given by the point spread function of the microscope.

Table 1. Renishaw 1000B μRaman Spectrometer Parameters

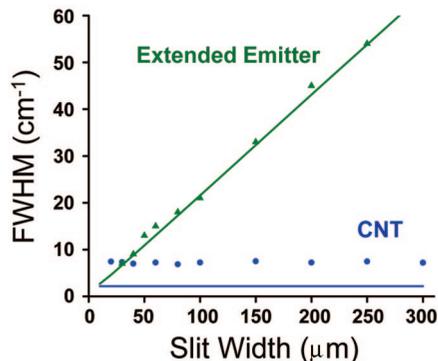| spectrometer parameters ($50\times$ objective)						$k = 1$, $\lambda_0 = 943$ nm		
L_{PreSlit} (mm)	M_{OS}	M_{SD}	L_B (mm)	n (g/mm)	pixel size (μm)	α (deg)	β (deg)	$d\sigma/dx$ (cm$^{-1}/\mu$m)
50	12.5	1.6	250	600	22	31.9	2.1	0.075

Figure 4. FWHM as a function of slit width. CNT G$^+$ Raman mode widths are shown in blue circles. Line widths of a spatially extended emitter (703.2 nm Ne line) are shown in green triangles. The system responses for macroscopic and point sources are shown with green and blue lines, as governed by eqs 2 and 4, respectively.

This is in stark contrast to spectroscopy from an extended source, e.g., monochromatic laser light from an extended area in the object plane will appear spectrally broad on the detector, unless a narrow spectrometer entrance slit in the intermediate image plane is used. The measured spectral width of a given feature from a macroscopic object depends on a convolution of the intrinsic line width, $\Delta\sigma_{int}$, with the instrument broadening which is given by the contribution from the widths of entrance slit and CCD pixel size, $\Delta\sigma_{slit}$ and $\Delta\sigma_{pixel}$.[29] Assuming Gaussian line profiles for a simple expression of the convolution,[30] we have

$$\Delta\sigma_{FWHM,macro} = \sqrt{\Delta\sigma_{int}^2 + \Delta\sigma_{slit}^2 + \Delta\sigma_{pixel}^2} \quad \text{(macroscopic source)} \quad (2)$$

where $\Delta\sigma_{pixel}$ gives the lowest instrument broadening if the slit is infinitely narrow. For a nanoscale emitter, the image size at the intermediate image plane slit is determined by the point spread function of the microscope objective, Δx_{PSF}, multiplied by the magnification M_{OS}. The intermediate image is magnified and mapped onto the detector and gives the contribution $\Delta\sigma_{PSF}$ to the spectral width

$$\Delta\sigma_{PSF} = \Delta x_{PSF} M_{OS} M_{SD} (W\prime_g/W\prime\prime_g)\, d\sigma/dx \quad (3)$$

where $W\prime_g/W\prime\prime_g = \cos(\alpha)/\cos(\beta)$ (Figure 1), so that

$$\Delta\sigma_{FWHM,nano} = \sqrt{\Delta\sigma_{int}^2 + \Delta\sigma_{PSF}^2 + \Delta\sigma_{pixel}^2} \quad \text{(point source)} \quad (4)$$

Note that it is the diffraction-limited point spread function that enters into the line width and that the line width is independent of the slit width.[31] Hence, a fully open slit does not contribute to a broadening of the line shape for a nanoscale emitter, in contrast to the case for spectroscopy of a macroscopic object, where a slit width larger than the corresponding pixel width always contributes to instrument broadening. The measured line width for the CNT emitter is shown in Figure 4 with blue circles using the 50×/0.5 NA objective. The solid blue line shows the contribution from the instrument resolution using eq 4 where $\Delta\sigma_{PSF}$ is approximated by the Rayleigh criterion. By removing this system contribution to the measured line width of 7.5 cm^{-1}, the intrinsic CNT Raman line width for the G band of a suspended nanotube is calculated to be 6.9 cm^{-1}. For

contrast, Figure 4 also shows, in green triangles, the measured line width from an atomically sharp transition (the Ne 703.2 nm line) where the line width is dominated by the system response due to the large physical extent of the source in the object plane. Specifically, the objective is focused on a 100 μm pinhole which is illuminated from below by a Ne lamp. The calculated line width contribution from the system for this case, as given by eq 2, is shown by the solid green line. Of course, in many cases, the emitter size is equal to the diffraction-limited laser spot size used to excite the sample and so the measured spectral line width dependence on slit width will fall somewhere between eqs 2 and 4.

In summary, using Raman scattering from an individual carbon nanotube, we have demonstrated that the spectral signature of a nanoemitter depends on the location relative to the optical axis along the direction perpendicular to the grating groves. The change in spectral signature is proportional to the total optical magnification and the linear dispersion of the spectrometer. Because the nanoemitter acts as a point source, the spectrometer entrance slit can be left open without negatively affecting the instrument line broadening, the "nanoslit" effect. However, a large open slit allows for larger shifts in measured spectral position. Finally, we demonstrate the use of a nanoemitter to measure the optical spot size of the microscope. We hope that these observations will be helpful for the growing nanospectroscopy community.

References
(1) Empedocles, S.; Bawendi, M. *Acc. Chem. Res.* **1999**, *32*, 389–396.
(2) Alen, B.; Bickel, F.; Karrai, K.; Warburton, R. J.; Petroff, P. M. *Appl. Phys. Lett.* **2003**, *83*, 2235–2237.
(3) Vamivakas, A. N.; Zhao, Y.; Lu, C.-Y.; Atature, M. arXiv:cond-mat/0806.3707.
(4) Bayer, M.; Ortner, G; Stern, O.; Kuther, A.; Gorbunov, A. A.; Forchel, A.; Hawrylak, P.; Fafard, S.; Hizner, K.; Reinecke, T. L.; Walck, S. N.; Reithmaier, J. P.; Klopf, F.; Schafer, F. *Phys. Rev. B* **2002**, *65*, 121309.
(5) Findeis, F.; Baier, M.; Zrenner, A.; Bichler, M.; Abstreiter, G.; Hohenester, U.; Molinari, E. *Phys. Rev. B* **2001**, *63*, 121309.
(6) Zrenner, A.; Markmann, M.; Paassen, A.; Efros, A. L.; Bichler, M.; Wegscheider, W.; Bohm, G.; Abstreiter, G. *Physica B* **1998**, *256*, 300–307.
(7) Cronin, S. B.; Yin, Y.; Walsh, A. G.; Capaz, R. B.; Stolyarov, A.; Tangney, P.; Cohen, M. L.; Louie, S. G.; Swan, A. K.; Ünlü, M. S.; Goldberg, B. B.; Tinkham, M. *Phys. Rev. Lett.* **2006**, *96*, 127403.
(8) Cronin, S. B.; Swan, A. K.; Ünlü, M. S.; Goldberg, B. B.; Dresselhaus, M. S.; Tinkham, M. *Phys. Rev. B* **2005**, *72*, 035425.
(9) Cronin, S. B.; Swan, A. K.; Ünlü, M. S.; Goldberg, B. B.; Dresselhaus, M. S.; Tinkham, M. *Phys. Rev. Lett.* **2004**, *93*, 167401.
(10) Lucas, M.; Young, R. J. *Phys. Rev. B* **2004**, *69*, 085405.
(11) Walsh, A. G.; Vamivakas, A. N.; Yin, Y.; Cronin, S. B.; Ünlü, M. S.; Goldberg, B. B.; Swan, A. K. *Nano Lett.* **2007**, *7*, 1485–1488.
(12) Walsh, A. G.; Vamivakas, A. N.; Yin, Y.; Cronin, S. B.; Ünlü, M. S.; Goldberg, B. B.; Swan, A. K. *Physica E* **2008**, *40*, 2375–2379.
(13) Advances are being made. See, e.g.: Arnold, M. S.; Green, A. A.; Hulvat, J. F.; Stupp, S. I.; Hersam, S. C. *Nat. Nanotechnol.* **2006**, *1*, 60–65.
(14) Zheng, M.; Jagota, A.; Strano, M. S.; Santos, A. P.; Barone, P.; Chou, S. G.; Diner, B. A.; Dresselhaus, M. S.; McLean, R. S.; Onoa, G. B.; Samsonidze, G. G.; Semke, E. D.; Usrey, M.; Walls, D. J. *Science* **2003**, *302*, 1545–1548.
(15) Reich, S.; Thomsen, C.; Maultzsch, J. *Carbon Nanotubes: Basic Concepts and Physical Properties*; Wiley-VCH: Berlin, 2004.

(16) We have found the nano-emitter to be helpful in correcting alignment issues and in diagnosing chromatic aberration effects arising from the beam waist not falling precisely at the plane of the slit. That is, the slit can begin to act as the system aperture stop.

(17) http://www.jobinyvon.com/SiteResources/Data/Templates/ 1divisional.asp?DocID=566&v1ID=&lang.

(18) Wang, F.; Sfeir, M. Y.; Huang, L.; Huang, X. M. H.; Wu, Y.; Kim, J.; Hone, J.; O'Brien, S.; Brus, L. E.; Heinz, T. F. *Phys. Rev. Lett.* **2006**, *96*, 167401.

(19) See Newport application note at http://www.newport.com/file_store/ Optics_and_Mechanics/AppsNote28.pdf.

(20) Wolf, E. *Phys. Rev. Lett.* **1987**, *58*, 2646–2648.

(21) Gbur, G.; Visser, T. D.; Wolf, E. *Phys. Rev. Lett.* **2002**, *88*, 013901.

(22) Jorio, A.; Souza Filho, A. G.; Brar, V. W.; Swan, A. K.; Ünlü, M. S.; Goldberg, B. B.; Righi, A.; Hafner, J. H.; Lieber, C. M.; Saito, R.; Dresselhaus, G.; Dresselhaus, M. S. *Phys. Rev. B* **2002**, *65*, 121402.

(23) The beam profile was determined by recording the power as a razor was advanced through the beam by micrometer screw, fitting the resulting curve with the error function, and taking the derivative. The results indicate an incident beam with a nearly perfect Gaussian profile. FWHM = 1.46 mm and objective back focal openings are 3.6 mm and 4 mm for the $100\times$ and $50\times$ objectives, respectively.

(24) Vamivakas, A. N.; Ippolito, S. B.; Swan, A. K.; Ünlü, M. S.; Dogan, M.; Behringer, E. R.; Goldberg, B. B. *Opt. Lett.* **2007**, *32*, 970–972.

(25) Rao, A. M.; Eklund, P. C.; Bandow, S.; Thess, A.; Smalley, R. E. *Nature* **1997**, *388*, 257–259.

(26) Tsang, J. C.; Freitag, M.; Perebeinos, V.; Liu, J.; Avouris, P. *Nat. Nanotechnol.* **2007**, *2*, 725–730.

(27) Novotny, L.; Hecht, B. *Principles of Nano-Optics*; Cambridge University Press: New York, 2006.

(28) This assumes scalar plane wave illumination of the back aperture in the paraxial limit for low NA and is actually a measure of the beam radius, not the FWHM. Hecht, E. *Optics*, 4th ed.; Addison Wesley: San Francisco, 2002.

(29) In most systems, the contribution from the grating resolution can be ignored. Here, $\Delta\sigma_g$ contributes <2% of the instrumental broadening.

(30) Here we use the Gaussian form to simply illuminate the different contributions to the line width even though the slit and the pixel have a rectangular form. The result in Figure 4 is obtained from a proper convolution.

(31) When the slit starts to clip the diffraction-limited spot size, the line-width contribution from the instrument response decreases. However, the system parameters are often chosen so that the pixel size is approximately commensurate with the diffraction-limited spot size at the slit making this effect moot.